

## Article

# Biomass Mediated Synthesis of ZnO and ZnO/GO for the Decolorization of Methylene Blue under Visible Light Source

Salma Ahmed Al-Zahrani <sup>1,\*</sup>, Khalid Umar <sup>2,\*</sup>, Saleh Ali Tweib <sup>3</sup>, Jebrel Abdeljawad M. Rashd <sup>4,5</sup>, Saima Khan Afridi <sup>2</sup>, Showkat Ahmad Bhawani <sup>6</sup>, Ahmed Al Otaibi <sup>1</sup>, Najat Masood <sup>1</sup>, Dorsaf Mansour <sup>1</sup>, Anish Khan <sup>7</sup>  and Manikandan Ayyar <sup>8</sup> 

<sup>1</sup> Chemistry Department, Faculty of Science, University of Ha'il, P.O. Box 2440, Ha'il 81451, Saudi Arabia

<sup>2</sup> School of Chemical Sciences, Universiti Sains Malaysia, Gelugor 11800, Pulau Pinang, Malaysia

<sup>3</sup> Chemical and Process Engineering, Zawia Higher Institute of Science and Technology-Central Zawia, Msehel 201300, Libya

<sup>4</sup> School of Industrial Technology, Universiti Sains Malaysia, Gelugor 11800, Pulau Pinang, Malaysia

<sup>5</sup> Chemical Engineering Department, Higher Institute of Science & Technology, Souq Khamis Emsihel, Tripoli 199002, Libya

<sup>6</sup> Faculty of Resource Science and Technology, Universiti Malaysia Sarawak, Kota Samarahan 94300, Sarawak, Malaysia

<sup>7</sup> Center of Excellence for Advanced Materials Research, King Abdulaziz University, Jeddah 21589, Saudi Arabia

<sup>8</sup> Department of Chemistry, Bharath Institute of Higher Education and Research (BIHER), Bharath University, Chennai 600073, Tamil Nadu, India

\* Correspondence: s.alzahrane@uoh.edu.sa (S.A.A.-Z.); khalidumar@usm.my (K.U.); Tel.: +60-46533567 (K.U.)

**Abstract:** In this study, zinc oxide (ZnO) as well as ZnO/GO (zinc oxide/graphene oxide) were successfully synthesized. The Carica papaya leaf extract was used to synthesize ZnO and oil palm empty fruit bunch biomass to obtain graphene, which was further used to obtain graphene oxide. The samples were characterized through a variety of analytical methods such as scanning electron microscopy, transmission electron microscopy, X-ray diffraction analysis, Fourier transform infrared spectroscopy and UV-Visible spectroscopy in order to understand their morphology, size, structural phase purity, functional groups and optical properties. Various peaks such as O-H, Zn-OH and Zn-O were found in the case of ZnO. Some additional peaks, such as C-C and C=C, were also been detected while analyzing the sample by Fourier-transform infrared spectroscopy. The results of the XRD and SEM studies demonstrated that the synthesized material shows the crystalline nature of the substance in the case of ZnO, and the crystallinity decreases for ZnO/GO. The average crystallite size was found to 80.0 nm for ZnO and 74.0 nm for ZnO/GO. Further, a red shift was shown in the case of ZnO/GO, which was indicated by the UV-Vis absorption spectrum. In the TEM analysis, the particles were shown to be nanosized. For instance, the highest number of particles was found in the range of 100 to 120 nm in the case of ZnO, while 80–100 nm sized particles were found for ZnO/GO. Using synthesized ZnO and ZnO/GO, the decolorization of methylene blue was found to be 64% and 91%, respectively.

**Keywords:** ZnO; ZnO/GO; photocatalyst; photodecolorization; green synthesis; methylene blue



**Citation:** Al-Zahrani, S.A.; Umar, K.; Tweib, S.A.; Rashd, J.A.M.; Afridi, S.K.; Bhawani, S.A.; Otaibi, A.A.; Masood, N.; Mansour, D.; Khan, A.; et al. Biomass Mediated Synthesis of ZnO and ZnO/GO for the Decolorization of Methylene Blue under Visible Light Source. *Catalysts* **2023**, *13*, 409. <https://doi.org/10.3390/catal13020409>

Academic Editors: Fengxia Deng and Xiaoxiao Zhang

Received: 11 December 2022

Revised: 30 January 2023

Accepted: 9 February 2023

Published: 14 February 2023



**Copyright:** © 2023 by the authors. Licensee MDPI, Basel, Switzerland. This article is an open access article distributed under the terms and conditions of the Creative Commons Attribution (CC BY) license (<https://creativecommons.org/licenses/by/4.0/>).

## 1. Introduction

Water pollution has threatened the survival of human beings, as many industries have been expelling harmful substances into the environment in recent decades [1–3]. Even though chemical compound-based companies have played an important role in modern life (especially those that make dyes, insecticides, pharmaceuticals, etc.), a lot of waste is thrown into the environment by them, which potentially disturbs our ecosystem on a continuous basis [4]. For instance, compounds which are soluble in water, such as pesticides, dyes, and drugs, are predominately accountable for contaminating aquatic

environments and have become a major cause of water pollution. These contaminants may also cause chronic diseases for human beings and are also harmful to our environment, even if they were present at very low levels. Therefore, the occurrence of such contaminants in water resources has emerged as a significant concern for environmental scientists [3,5]. In addition, several pesticides, drugs, and dyes have already been reported in various water resources across the globe in groundwater and surface water due to various types of activities [6–8]. Among them, dyes are producing a high level of water pollution, as yearly 70,000 tons is manufactured globally and 12% of these dyes are lost during the dying process in color industries, which eventually leads to the obliteration of our aquatic system [6,9]. Therefore, it is necessary to remove/degrade such pollutants from the polluted water before releasing them into the water sources.

The photocatalytic degradation method has emerged as a feasible process for the elimination of different pollutants from the aqueous solution. To address this issue, in the past several years various photocatalysts such as ZnO, TiO<sub>2</sub>, etc, have been used [10–13]. Among them, ZnO is considered a prominent photocatalyst because of its higher stability, while irradiation is inexpensive, and has low toxicity [14]. Nevertheless, despite these benefits, the single semiconductor has certain drawbacks as it exhibits low photocatalytic activity in visible light because of its high bandgap energy [10,15]. The band gap energy was calculated for ZnO (3.3 eV), which demonstrates that it was only capable of absorbing close-ultraviolet light ( $\lambda < 387$  nm) but is not suitable for working in visible light regions [13]. Therefore, there is a need for doing the necessary modifications to make it fit for working in the visible range.

Conversely, graphene derivatives are gaining considerable attention because their structure makes them ideal building blocks for a wide variety of novel applications such as photocatalysts [16], biosensors [17], batteries [18], and supercapacitors [19]. Moreover, because of graphene oxide's mechanical, electric, thermal, and optical properties, it has also been considered a material platform in modern technology. The properties of these materials can be modified through the application of a simple chemical functionalization process [20,21]. There have also been a number of publications in recent years that discuss the combination of ZnO with graphene oxide as a means of degrading a variety of pollutants [22–26]. Additionally, the synthesizing of ZnO in different sizes and shapes has been attempted using a variety of techniques, including hydrothermal, chemical microemulsion, wet chemical, sol-gel, direct precipitation, vapor phase, solvothermal, microwave, and sonochemical techniques [27,28]. However, a high amount of chemicals has been used while applying these techniques in the process of synthesis. Therefore, a simple and less chemically oriented method is still needed for the preparation of photocatalysts.

There has been much attention given to green synthesis methods for the preparation of metal oxides because they offer many advantages over chemical methods (non-green). The benefits of this synthesis environment include simplicity, energy efficiency, eco-friendliness, and low toxic levels [29]. Thus, there are many articles that report on synthesizing ZnO via the green synthesis method. For instance, the synthesis of ZnO using coffee powder as a photocatalyst [30,31]. In addition, plant extracts of *Physalis alkekengi* L. and *Sedum Alfredii* Hance were also used to synthesize crystalline ZnO [32,33]. As far as the extract of papaya leaf is concerned, which was used in this study, it contains many flavonoid and phenolic compounds with reducing and stabilizing properties that may play an important role in metal oxide synthesis [34–38].

Furthermore, the synthesis of graphene oxide using biomass such as agro-waste can also be considered a good idea to prepare a valuable compound as well as to reduce the waste from the environment, as few studies have been reported in the literature [39–42]. Hence, in the present work, we reported a green synthesis of zinc oxide (ZnO) using *Carica papaya* leaf extract. Moreover, the oil palm empty fruit bunch biomass was utilized to obtain graphene, which was further employed for the formation of graphene oxide. The synthesized ZnO/GO (zinc oxide/graphene oxide) was able to work as a photocatalyst active in visible light. There are some techniques that were used in the current work to

characterize the synthesized material, and the photocatalytic performance was investigated by degrading methylene blue (dye).

## 2. Results and Discussion

### 2.1. SEM Analysis

Scanning Electron Microscopy (SEM) was employed in order to investigate the morphology of ZnO and ZnO/GO. Figure 1a,b describe the morphology of ZnO and ZnO/GO, respectively. The crystalline nature of ZnO can be seen in the SEM image of ZnO, while in the case of ZnO/GO, with some modification, zinc oxide particle could be seen on GO. Moreover, the ZnO/GO catalyst also shows a cross-linked amorphous structure; however, the dispersibility of particles were found to be excellent without agglomeration.

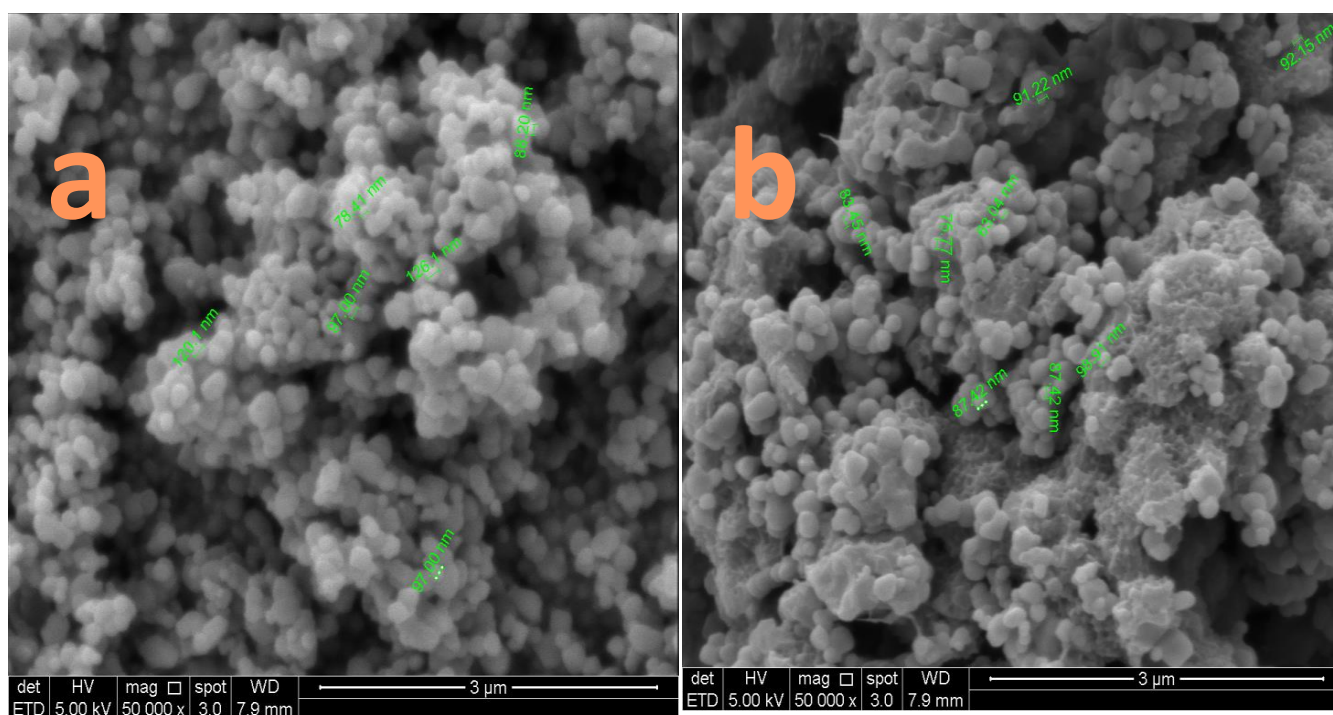


**Figure 1.** SEM image of ZnO (a) and ZnO/GO (b).

### 2.2. TEM Analysis

Transmission Electron Microscopy (TEM) was used for ZnO and ZnO/GO and the results of this investigation are depicted in Figure 2a,b. TEM images provided evidence of the nanoscale range and a homogeneous distribution of the particles. Moreover, nanoparticle aggregations do not appear in any of these images, which is an additional significant quality of the synthesized material. Furthermore, Figure 2c,d demonstrated the particle distribution pattern of ZnO and ZnO/GO, respectively. The maximum number of particles were found in the range of 100 to 120 nm in the case of ZnO, while the 80–100 nm size was found for ZnO/GO, which could also account for the better photocatalytic performance [21].

### 2.3. XRD Analysis

The XRD spectra results for ZnO and ZnO/GO were shown in Figure 3a,b. Figure 3a depicts the results of an XRD analysis, showing the crystalline nature of ZnO, while in the case of ZnO/GO crystallinity decreases to some extent. The peaks at dispersion inclinations (2 theta) of 32, 34.6, 36.4, 47.8, 56.8, 63, 66.6, 68 and 69.2 are detected for ZnO and well indexed to the hexagonal phase for ZnO, as reported in JCPDS card number 36–1451 [13,37]. These peaks correspond to the reflection from the crystal planes (100), (002), (101), (102), (110), (103), (200), (112) and (201), respectively.

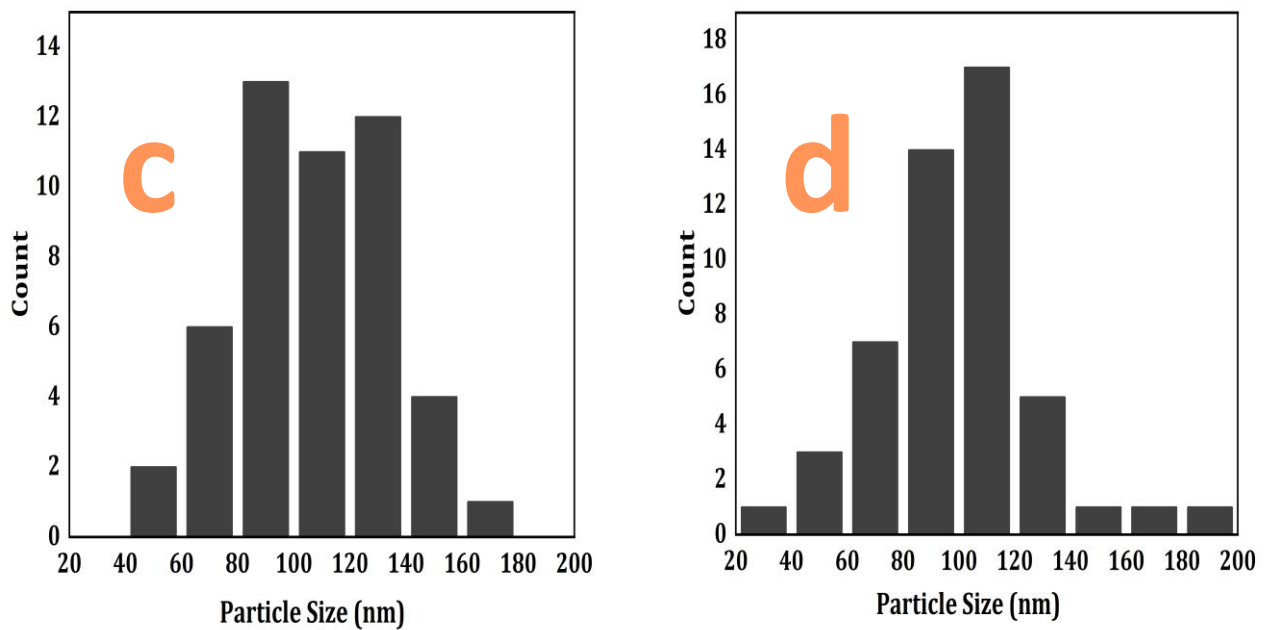
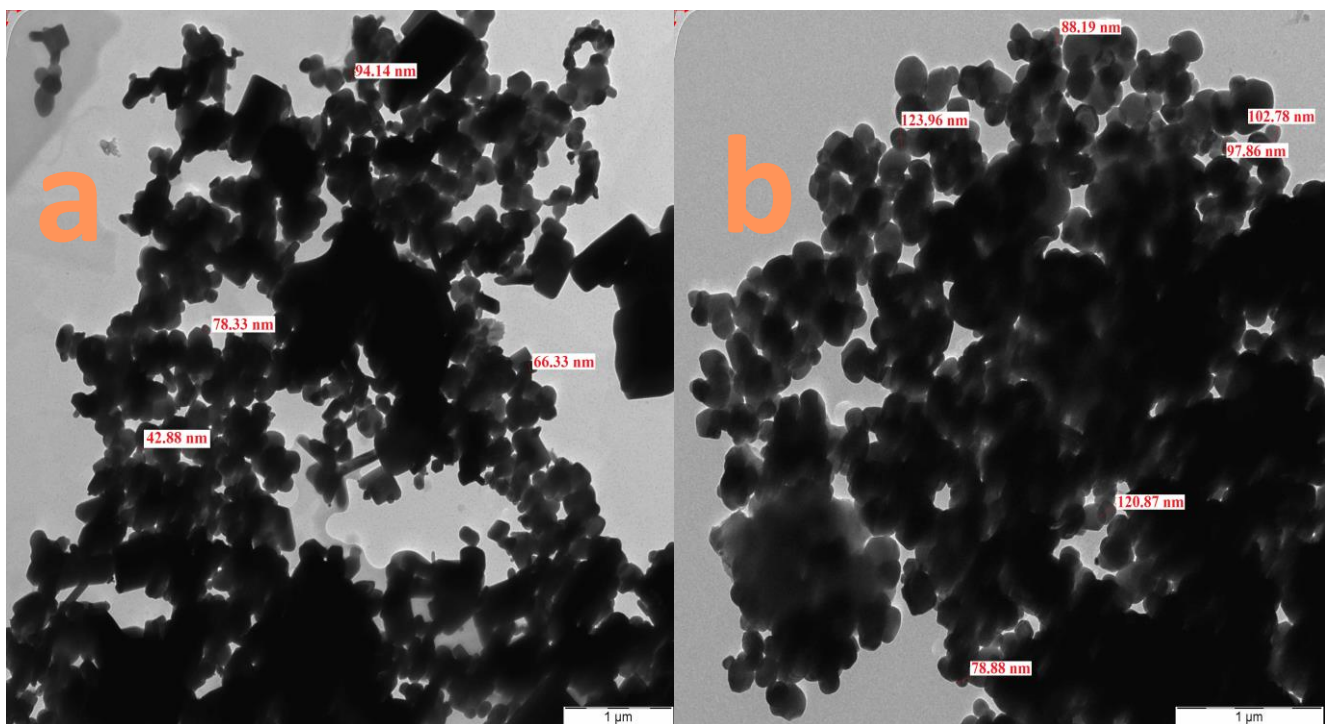


Figure 2. TEM images of ZnO (a) and ZnO/GO (b). Particle size distribution histograms for ZnO (c,d).

As can be seen in Figure 3b, a peak appears roughly at 10 (with a scattering angle of 2 theta), which corresponds to graphene oxide [42]. Moreover, no considerable shifting of other peaks is observed in the case of ZnO/GO. The average crystallite size of ZnO was governed by the Scherrer equation (Equation (1)), and was found to be 80.0 nm (ZnO) and 74.0 nm (ZnO/GO).

$$D = \frac{K\lambda}{\beta \cos \theta} \quad (1)$$

where  $D$  = crystallite size,  $K$  = shape factor,  $\lambda$  = wavelength,  $\theta$  = diffraction angle,  $\beta$  = full width at half maximum.

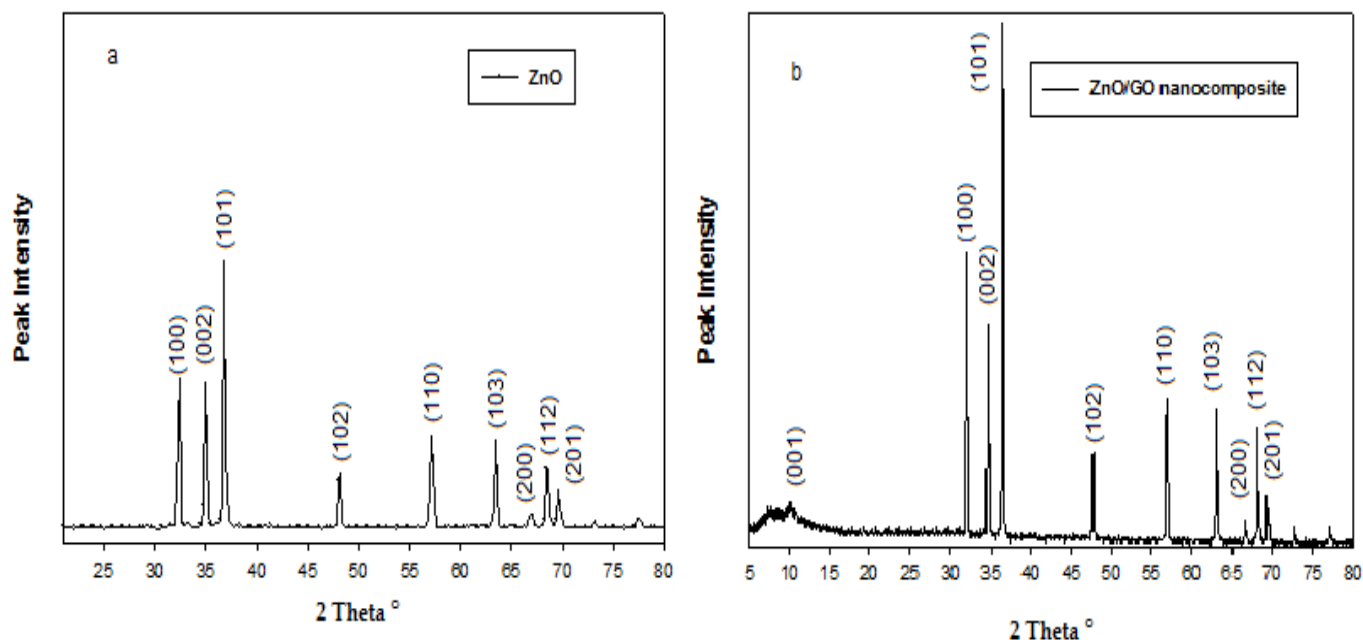


Figure 3. XRD patterns of ZnO (a) and ZnO/GO (b).

#### 2.4. UV–Visible Absorption Spectra

As shown in Figure 4a,b, the UV–Visible absorption spectra of ZnO and ZnO/GO were measured. In this study, band gap energies for nanocomposite systems of ZnO and ZnO/GO were determined using Equation (2). Based on the absorbance data collected from these figures, the band gap energy was calculated [43,44].

$$\text{Band gap (eV)} = 1240/(\text{wavelength}) \text{ (nm)} \quad (2)$$

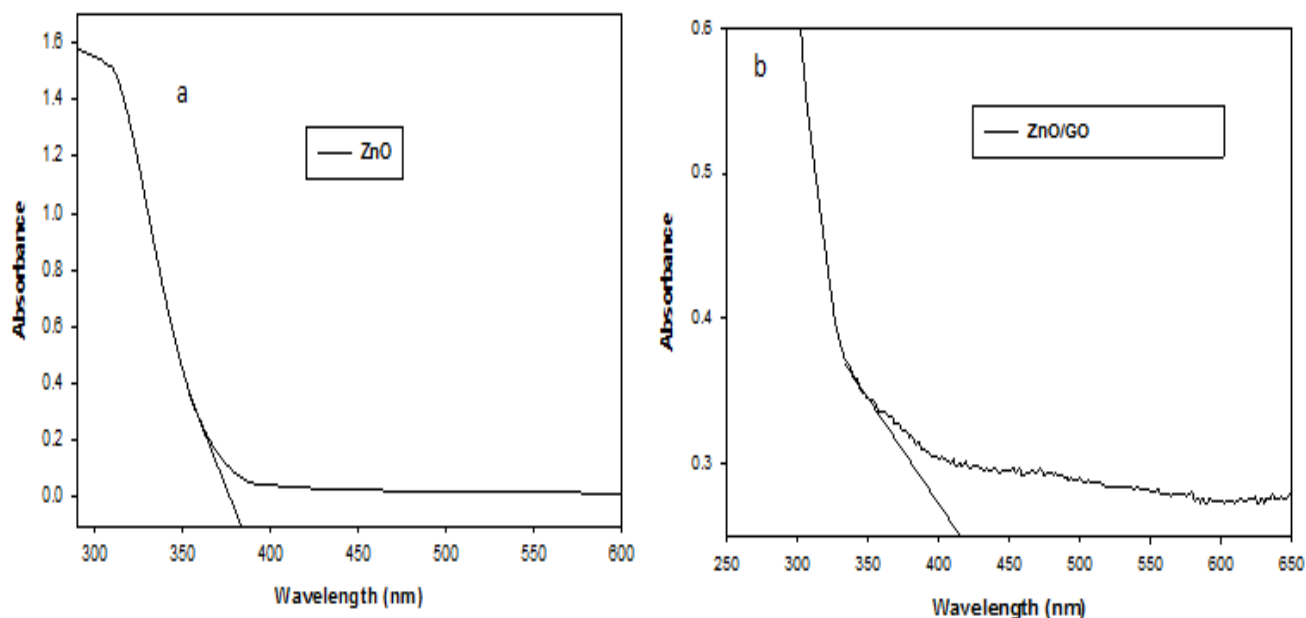


Figure 4. ZnO absorption spectrum (a) and ZnO/GO absorption spectrum (b).

ZnO and ZnO/GO were found to have bandgap energies of 3.16 eV and 2.99 eV, respectively. In the case of ZnO/GO, a shifting of the absorption edge towards the higher wavelength could be seen in Figure 4b, meaning a decrease in the value of band gap energy [45,46]. Furthermore, this meant that the formation of this heterojunction between ZnO and graphene oxide is responsible for the photoresponse in the visible region. In

addition, this reduction in band energy was found to be helpful to work the photocatalyst in the visible range of light. These findings are in great accordance with previous studies (12, 15, 43, 44).

### 2.5. FTIR Analysis

Figure 5 demonstrates the findings of an FTIR spectrum assessment that was accomplished for the purpose of the evaluation of functional groups for ZnO and ZnO/GO. Because of the stretching and going-to-bend vibration of OH groups, GO exhibited a wide peak at 3100 and 3600  $\text{cm}^{-1}$  and a sharp peak was observed at 1626  $\text{cm}^{-1}$  [47]. It is conceivable that this was caused by the appearance of water molecules that had been trapped in GO. It is also possible that the symmetric and anti-symmetric stretching of C-H to the absorption peaks may be found in the mid-frequency region at 2750  $\text{cm}^{-1}$  and 2830  $\text{cm}^{-1}$ , respectively. The values found in the literature have been consistent with the ZnO frequencies that were discovered through infrared study [48–50]. A fingerprint absorption zone may be found below 1000  $\text{cm}^{-1}$ , due to the inter-atomic vibrations that occur in metal oxide. The appearance of peaks at 3450  $\text{cm}^{-1}$  demonstrates that water molecules may be adsorbed onto the zinc surface. In addition, a widening of the peak was observed in the scenario of ZnO/GO, which may be caused by the interaction between two components, specifically ZnO and GO [48].

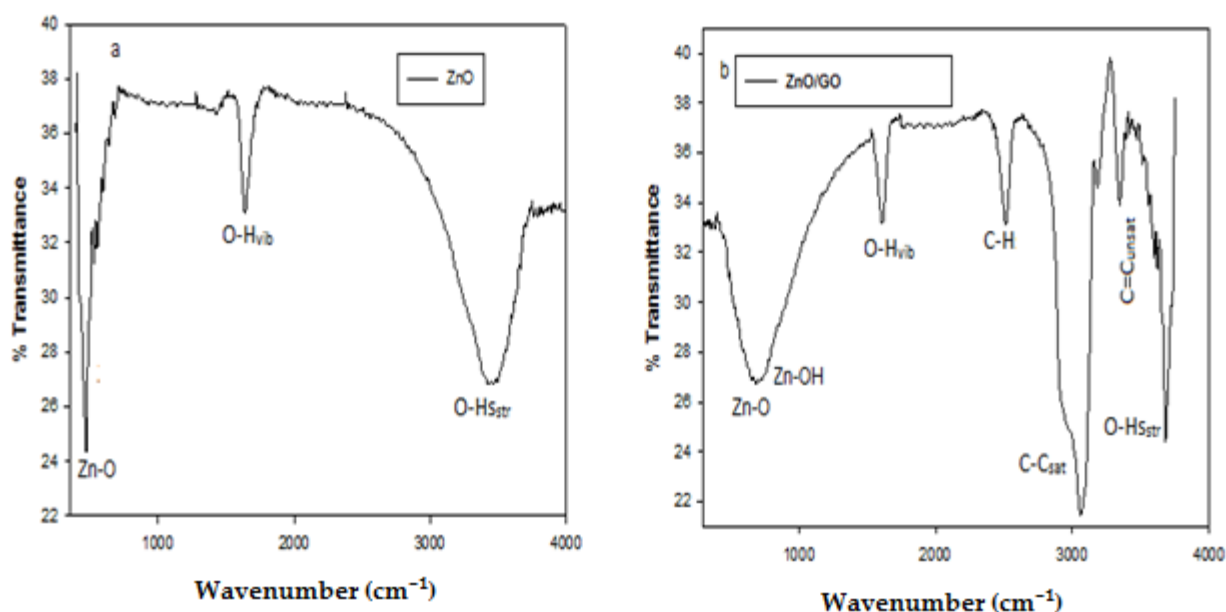


**Figure 5.** FTIR spectra of ZnO (a) and ZnO/GO (b).

### 2.6. Photoluminescence Spectroscopy (PL)

Figure 6 illustrates the results of the photoluminescence intensity for ZnO and ZnO/GO. As the recombination of stimulated holes and electrons is strongly associated with the PL emission, a smaller value of the obtained peak suggests a delay in the rate of recombination and, as a result, photocatalytic activity will be better. It is, additionally, owing to better charge movement at the interface and decreased electron recombination, which suggests that photoinduced electrons produced in ZnO are quickly moved to GO [29,49–52]. The layer of GO performs the function of an electron sink, providing an alternative pathway for the separation of charge carriers.

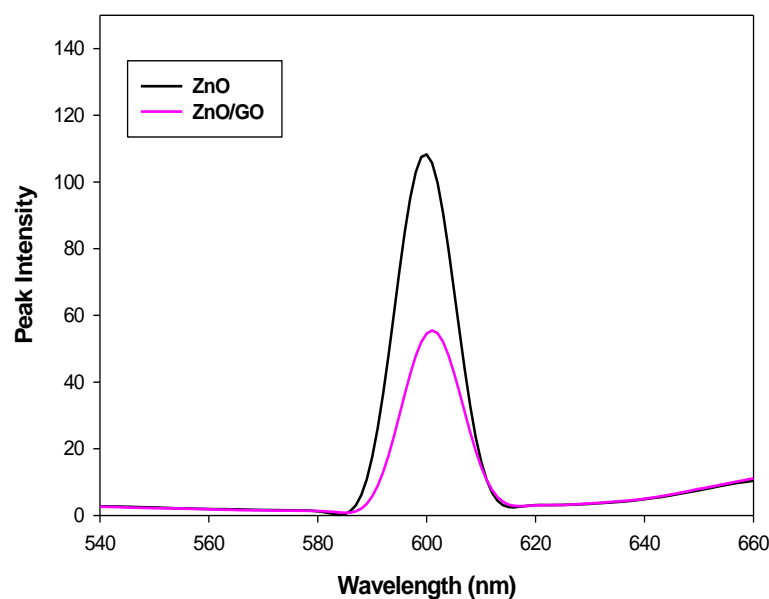


Figure 6. PL spectra of ZnO and ZnO/GO.

### 3. Photocatalytic Activity

#### 3.1. A study of Photocatalysis of Methylene Blue in the Presence of Nanocomposites ZnO and Zn/GO

In an irradiation experiment, an aqueous solution (250 mL) of methylene blue (0.30 M) was irradiated with a visible light halogen lamp. The concentration of photocatalysts (ZnO and ZnO/GO) was  $1 \text{ gL}^{-1}$ . Throughout this process, the solution was continuously stirred and atmospheric oxygen was supplied by using an air pump. By utilizing the absorbance as a function of the irradiation time, the degradation process of the dye was observed. The analogous condition was applied in the case of the ZnO/GO, too. Figures 7 and 8 demonstrate the variation in absorbance that occurs at various time intervals as a result of the irradiation of methylene blue in the existence of ZnO and ZnO/GO, respectively. It is obvious that the intensity of the irradiation's absorption decreases with an increase in the exposure time, as is shown in the figures.

The change in the initial dye concentration ( $C/C^0$ ) as a function of the irradiation time was depicted in both conditions, the presence and absence of ZnO and ZnO/GO nanocomposites, as shown in Figure 9 [12]. When ZnO was irradiated with Methylene Blue for 80 min, 64% of the dye was removed; however, in the case of ZnO/GO nanocomposite, 91% of the decolorization was observed. On the other hand, if there was no photocatalyst available then there was no detectable reduction in the concentration of the dye. The reason for this efficient activity may be due to the decrease in the band gap that results from the formation of the heterojunction of ZnO and GO, which may be attributable to the fact that the material is able to absorb light with longer wavelengths, i.e., visible region [21]. The heterojunction formation with ZnO and GO also affect the life of charge carriers by trying to delay the time through which photogenerated holes and electrons reach the surface of the photocatalyst [50].

#### 3.2. Reusability of the Photocatalyst

The reusability of the synthesized nanocomposites of GO/ZnO has been assessed in order to study the performance and reliability, durability, operational stability, and effectiveness of the particles. Filtration has been performed to retrieve the catalyst, so that it could be utilized in continuing to follow reusability process. The decolorization of methylene blue following recycling four times has been observed to be retained at 89% (only 2% was decreased, as compared to the original value after four cycles), and as shown in Figure 10, GO/ZnO exhibits a very high degree of stability during the photocatalytic

degradation process. A study performed by Chuhan et al. [53], also observed the same results; that is, a decrease (small) in the effectiveness of degradation might result from the accumulation of specific oxidation products at the surface of the catalyst, which has the effect of limiting multiple active catalysts zones. Moreover, the strong redox capability of the substance additionally enables it to produce remarkable reducing efficiency for the organic pollutants at smaller concentrations. As a result, the GO/ZnO nanocomposite has the potential to be of practical application in the elimination of contaminants with the help of a catalyst using visible-light-responsive.

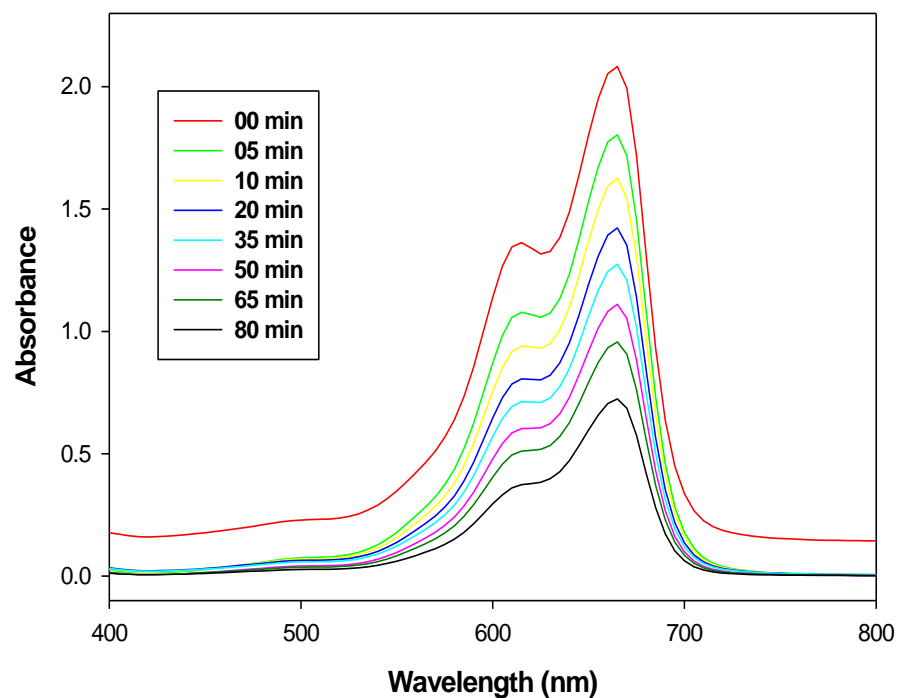


Figure 7. An absorption spectrum for methylene blue decolorization in the presence of zinc oxide.

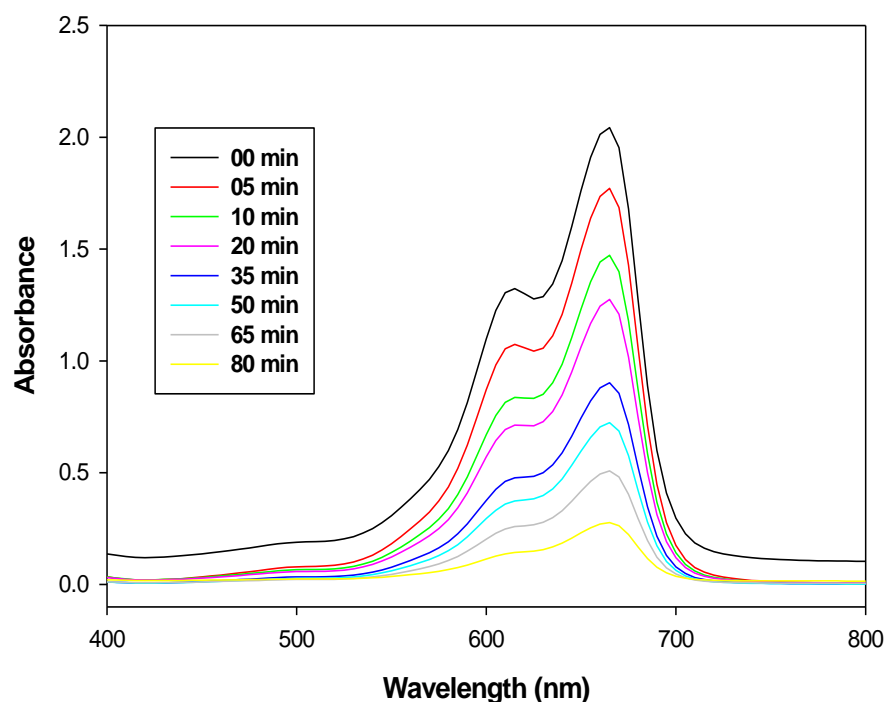
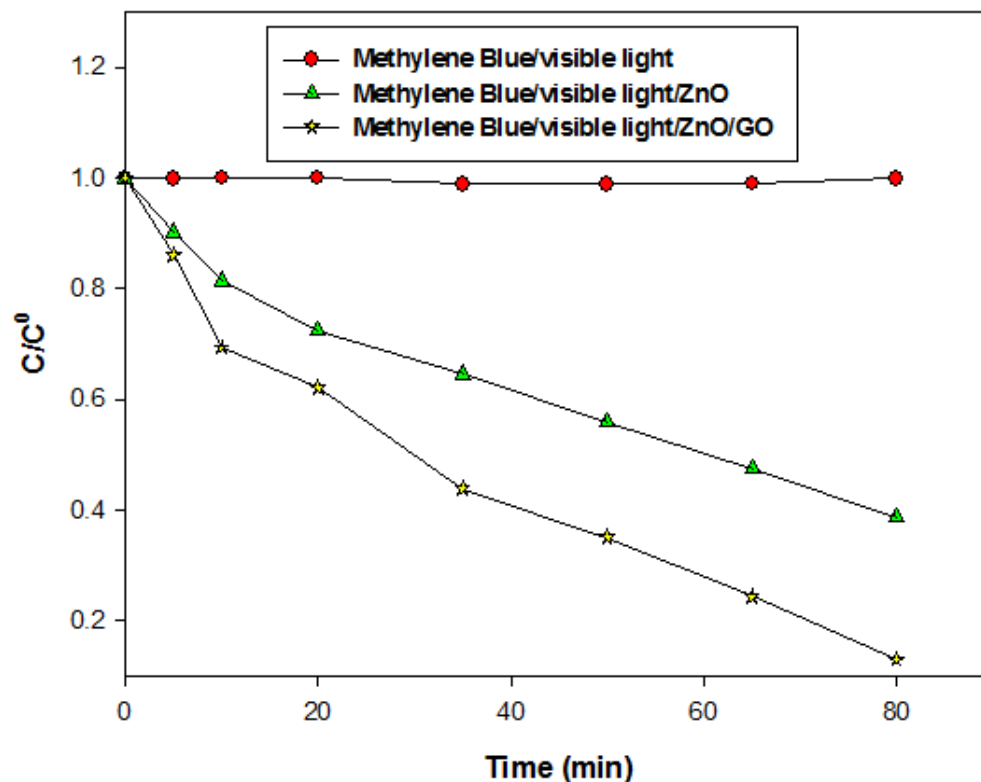
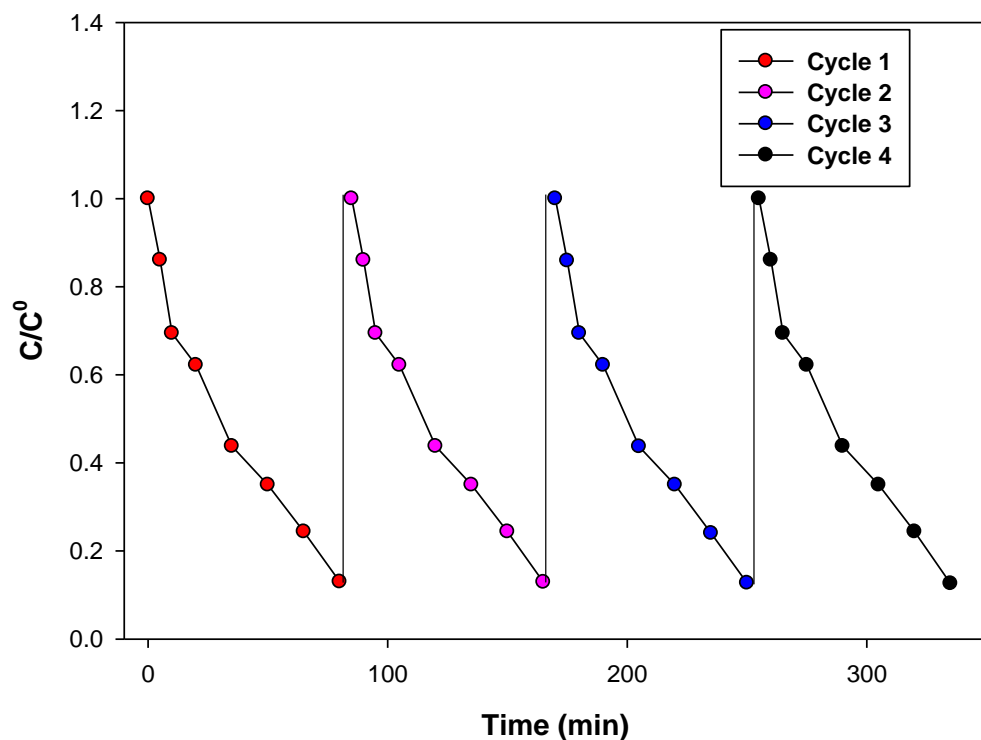


Figure 8. An absorption spectra for methylene blue decolorization in the presence of ZnO-GO.



**Figure 9.** Observation of changes in methylene blue concentration with time following irradiation in the absence and presence of ZnO and ZnO/GO.



**Figure 10.** Reusability of ZnO-GO nanocomposite for the decolorization of methylene blue.

#### 4. Material and Methods

##### 4.1. Chemical Reagents

Herewith, oil palm empty fruit bunch received from Sabutek (M) Sdn. Bhd, Malaysia and papaya leaves collected from the main campus of Universiti Sains Malaysia (USM),

which is located at Penang (Malaysia), were used in this study. Moreover, sodium nitrate, potassium permanganate (Sigma-Aldrich), 99% of hydrochloric acid (AR grade; QRec), ammonium persulfate (R & M chemicals), 30–32% of hydrogen peroxide (QRec), 95–97% of sulfuric acid (QRec) and >99.5% of zinc acetate dihydrate (Merck) were also used.

#### 4.2. Synthesis of ZnO

In this study, zinc oxide synthesis and extraction of papaya leaf were carried out according to [29], with some modification. Briefly, firstly 50 g of papaya leaf was taken and carefully chopped. In the next step, distilled water (10 mL) was added and then it was refluxed at 100 °C for 60 min before being filtered through the Whatman filter paper. Subsequently, ZnO was synthesized with the help of the papaya leaf extract that was prepared. A typical ZnO synthesis involves adding 15 mmol of zinc acetate dihydrate (>99.5%, Merck) to 75 mL of distilled water, followed by 30 min of the solution sonication. After that, 50 mL extract of papaya leaf was added to the solution with continuous stirring, and the solution temperature was fixed at 70 °C throughout the process. In the end, the white color precipitate was obtained and, after washing with ethanol and water, it was centrifuged. Finally, it was dried at 85 °C for 15 h.

#### 4.3. Preparation of Carbonized Carbon and Synthesis of ZnO/GO Nanocomposite

The biomass (empty fruit bunches of oil palm) was chopped into little pieces and then put in the furnace for 3 h at 700 °C. After the carbonization process, the carbon flakes were pulverized into a fine powder before the oxidation process of the GO synthesis. A modified Hummer's method was applied to prepare GO from the carbonized material [42]. During the preparation process, 5 g of the carbonized carbon powder and 6 g of sodium nitrate were treated with sulfuric acid for 1 h. As a result of stirring continuously for 3 h at 0–5 °C with the continuous addition of potassium permanganate, a violet-brown colored material was obtained.

The mixture was then added with constant stirring to 150 mL of distilled water, until it was dark brown in color. Moreover, the temperature was maintained at 90–120 °C throughout this process. Then, the mixture was cooled down to room temperature in order to decrease the impact of the potassium permanganate. After that, 200 mL water was added, followed by a 30 mL solution of hydrogen peroxide. Later, the solution of zinc acetate dihydrate and the papaya leaf extract was added drop wise to the above solution with continuous stirring. Afterward, the ZnO/GO material was obtained by filtering out and rinsing it many times with water. Finally, a powder was collected after keeping it in an oven at 100 °C for 24 h. Figure 11 illustrates the systematic synthesis of ZnO and ZnO/GO nanocomposite using green chemistry.

#### 4.4. Material Characterization

The synthesized material was investigated using different techniques in terms of its morphological, structural, and optical characteristics. For instance, the scanning electron microscope (SEM) (Quanta FEG 650, Fei; Columbia, MO, USA), X-Ray diffraction (XRD) (Philips PW 1710 X-ray diffractometer; New York, NY, USA), UV–Visible spectrophotometer (Shimadzu UV–Vis 1601), fluorescence spectrometer (Perkin Elmer LS 55) with excitation wavelength 350 nm, Fourier transform infrared (FTIR) (Perkin Elmer model System 2000; Norwalk, CT, USA) and the transmission electron microscope (TEM) (Model Zeiss Libra 120; Jena, Germany) were applied to obtain the characteristics/properties of the synthesized material in this study. Especially, for TEM analysis, a beam of electrons interacts with the sample and forms a picture of the sample on a photographic plate. As a consequence, the sample must be capable of sustaining electrons in a vacuum chamber. TEM requires ultra-thin samples, so preparing samples for TEM is a time-consuming process. Firstly, the pinch of the sample was dispersed in solvent, and with the help of a dropper one drop of the dispersed sample was deposited onto support grid. By applying plastic embedding, the particles were fixed to facilitate the handling of the sample.



Figure 11. A systematic diagram showing the green synthesis method for ZnO and ZnO/GO.

#### 4.5. Photocatalytic Experiments

In order to examine the photocatalytic properties of synthesized materials, Pyrex glass photochemical reactors were used. For this purpose, the required amount of methylene blue (MB, 0.30 M) was added to distilled water to make a solution. Aqueous solutions of dye and photocatalyst ( $1 \text{ gL}^{-1}$ ) were placed in the reactor to carry out the irradiation experiments. Throughout the period of the experiment, the solution was stirred (250 rpm) continuously in the presence of oxygen. Before starting the irradiation process, the system was stirred for at least 15 min. Later, the irradiation was carried out with the help of a visible light halogen lamp that possessed 500 W (9500 Lumens). During the irradiation process, the samples were taken at certain intervals of time with the help of a syringe. Then, the solution was centrifuged and analyzed by using a UV–VIS spectrophotometer.

## 5. Conclusions

Biomass-mediated syntheses of zinc oxide (ZnO) and zinc oxide/graphene oxide (ZnO/GO) have been successfully achieved. Carica papaya leaf extract was used to synthesize ZnO. The crystalline (ZnO) and partially crystalline nature (ZnO/GO) were found in the analysis by XRD and SEM. The nano range of synthesized materials were confirmed with TEM results and the average crystallite size was found to be 80.0 nm for ZnO and 74.0 nm for ZnO/GO, while regarding the formation of heterojunction of ZnO/GO, the UV–Visible absorption spectra showed  $\lambda_{\text{max}}$  shift towards a longer wavelength. Furthermore, the obtained peaks for FTIR are also in good agreement with the synthesized materials. The smaller value of the obtained peak in the case of ZnO/GO suggests a delay in the rate of recombination, which supports the better photocatalytic activity. The photocatalytic activity of ZnO/GO showed high efficiency when compared to ZnO for the decolorization of the dye, i.e., a 64% decolorization of methylene blue took place in the presence of ZnO after 80 min of irradiation, whereas in the presence of ZnO/GO a 91% decolorization was observed. Furthermore, the reusability test also confirms the goodness and stability of ZnO/GO.

**Author Contributions:** Conceptualization, K.U.; methodology, S.K.A.; software, A.K.; investigation, S.A.A.-Z.; resources, S.A.B.; writing—original draft preparation, K.U.; writing—review and editing, S.A.T.; J.A.M.R.; A.A.O.; N.M.; D.M.; M.A. supervision, K.U.; funding acquisition, S.A.A.-Z. All authors have read and agreed to the published version of the manuscript.

**Funding:** This research has been funded by Scientific Research Deanship at University of Ha'il, Saudi Arabia through project number RG-21 032.

**Data Availability Statement:** Data can be provided on the request from the corresponding author.

**Conflicts of Interest:** The authors declare no conflict of interest.

## References

1. Bouwer, H. Integrated water management for the 21st century: Problems and solutions. *J. Irrig. Drain. Eng.* **2002**, *128*, 193–202. [[CrossRef](#)]
2. Anju, A.; Ravi, S.P.; Bechan, S. Water pollution with special reference to pesticide contamination in India. *J. Water Resour. Prot.* **2010**, *2*, 432–448.
3. Arora, N.K.; Fatima, T.; Mishra, I.; Verma, M.; Mishra, J.; Mishra, V. Environmental sustainability: Challenges and viable solutions. *Environ. Sustain.* **2018**, *1*, 309–340. [[CrossRef](#)]
4. Teh, C.M.; Mohamed, A.R. Roles of titanium dioxide and ion-doped titanium dioxide on photocatalytic degradation of organic pollutants (phenolic compounds and dyes) in aqueous solutions: A review. *J. Alloys Compd.* **2011**, *509*, 1648–1660. [[CrossRef](#)]
5. Begam, B.F.; Kumar, J.S. A study on cheminformatics and its applications on modern drug discovery. *Procedia Eng.* **2012**, *38*, 1264–1275. [[CrossRef](#)]
6. Umar, K.; Dar, A.A.; Haque, M.M.; Mir, N.A.; Muneer, M. Photocatalysed decolourization of two textile dye derivatives, Martius yellow and acid blue 129, in UV-irradiated aqueous suspensions of titania. *Desalin. Water Treat.* **2012**, *46*, 205–214. [[CrossRef](#)]
7. Chau, N.D.G.; Sebesvari, Z.; Amelung, W.; Renaud, F.G. Pesticide pollution of multiple drinking water sources in the Mekong Delta, Vietnam: Evidence from two provinces. *Environ. Sci. Pollut. Res.* **2015**, *22*, 9042–9058. [[CrossRef](#)]
8. Omran, E.-S.E.; Negm, A. Impacts of pesticides on soil and water resources in Algeria. In *Water Resources in Algeria-Part I*; Springer: Berlin/Heidelberg, Germany, 2020; pp. 69–91.
9. Neppolian, B.; Choi, H.C.; Sakthivel, S.; Arabindoo, B.; Murugesan, V. Solar/UV-induced photocatalytic degradation of three commercial textile dyes. *J. Hazard. Mater.* **2002**, *89*, 303–317. [[CrossRef](#)]
10. Sano, T.; Puzenat, E.; Guillard, C.; Geantet, C.; Matsuzawa, S. Degradation of C<sub>2</sub>H<sub>2</sub> with modified-TiO<sub>2</sub> photocatalysts under visible light irradiation. *J. Mol. Catal. A Chem.* **2008**, *284*, 127–133. [[CrossRef](#)]
11. Umar, K.; Haque, M.M.; Mir, N.A.; Muneer, M.; Farooqi, I.H. Titanium dioxide-mediated photocatalysed mineralization of two selected organic pollutants in aqueous suspensions. *J. Adv. Oxid. Technol.* **2013**, *16*, 252–260. [[CrossRef](#)]
12. Umar, K.; Haque, M.M.; Muneer, M.; Harada, T.; Matsumura, M. Mo, Mn and La doped TiO<sub>2</sub>: Synthesis, characterization and photocatalytic activity for the decolourization of three different chromophoric dyes. *J. Alloys Compd.* **2013**, *578*, 431–438. [[CrossRef](#)]
13. Umar, K.; Aris, A.; Parveen, T.; Jaafar, J.; Majid, Z.A.; Reddy, A.V.B.; Talib, J. Synthesis, characterization of Mo and Mn doped ZnO and their photocatalytic activity for the decolorization of two different chromophoric dyes. *Appl. Catal. A Gen.* **2015**, *505*, 507–514. [[CrossRef](#)]
14. Liu, S.; Liu, X.; Chen, Y.; Jiang, R. A novel preparation of highly active iron-doped titania photocatalysts with Ap-n junction semiconductor structure. *J. Alloys Compd.* **2010**, *506*, 877–882. [[CrossRef](#)]
15. Raza, W.; Haque, M.M.; Muneer, M.; Fleisch, M.; Hakki, A.; Bahnemann, D. Photocatalytic degradation of different chromophoric dyes in aqueous phase using La and Mo doped TiO<sub>2</sub> hybrid carbon spheres. *J. Alloys Compd.* **2015**, *632*, 837–844. [[CrossRef](#)]
16. Xiang, Q.; Yu, J.; Jaroniec, M. Graphene-based semiconductor photocatalysts. *Chem. Soc. Rev.* **2012**, *41*, 782–796. [[CrossRef](#)] [[PubMed](#)]
17. Zhu, C.; Fang, Y.; Wen, D.; Dong, S. One-pot synthesis of functional two-dimensional graphene/SnO<sub>2</sub> composite nanosheets as a building block for self-assembly and an enhancing nanomaterial for biosensing. *J. Mater. Chem.* **2011**, *21*, 16911–16917. [[CrossRef](#)]
18. Hsieh, C.-T.; Lin, C.-Y.; Chen, Y.-F.; Lin, J.-S. Synthesis of ZnO@Graphene composites as anode materials for lithium ion batteries. *Electrochim. Acta* **2013**, *111*, 359–365. [[CrossRef](#)]
19. Wang, H.; Yang, Y.; Liang, Y.; Robinson, J.T.; Li, Y.; Jackson, A.; Cui, Y.; Dai, H. Graphene-wrapped sulfur particles as a rechargeable lithium-sulfur battery cathode material with high capacity and cycling stability. *Nano Lett.* **2011**, *11*, 2644–2647. [[CrossRef](#)]
20. Kim, J.; Cote, L.J.; Huang, J. Two dimensional soft material: New faces of graphene oxide. *Acc. Chem. Res.* **2012**, *45*, 1356–1364. [[CrossRef](#)]
21. Boukhoubza, I.; Khenfouch, M.; Achehboune, M.; Leontie, L.; Galca, A.C.; Enculescu, M.; Carlescu, A.; Guerboub, M.; Mothudi, B.M.; Jorio, A.; et al. Graphene oxide concentration effect on the optoelectronic properties of ZnO/GO nanocomposites. *Nanomaterials* **2020**, *10*, 1532. [[CrossRef](#)]
22. Khan, M.; Tahir, M.N.; Adil, S.F.; Khan, H.U.; Siddiqui, M.R.H.; Al-warthan, A.A.; Tremel, W. Graphene based metal and metal oxide nanocomposites: Synthesis, properties and their applications. *J. Mater. Chem. A* **2015**, *3*, 18753–18808. [[CrossRef](#)]
23. Atchudan, R.; Edison, T.N.J.I.; Perumal, S.; Shanmugam, M.; Lee, Y.R. Direct solvothermal synthesis of zinc oxide nanoparticle decorated graphene oxide nanocomposite for efficient photodegradation of azo-dyes. *J. Photochem. Photobiol. A Chem.* **2017**, *337*, 100–111. [[CrossRef](#)]
24. Atchudan, R.; Edison, T.N.J.I.; Perumal, S.; Karthikeyan, D.; Lee, Y.R. Facile synthesis of zinc oxide nanoparticles decorated graphene oxide composite via simple solvothermal route and their photocatalytic activity on methylene blue degradation. *J. Photochem. Photobiol. B Biol.* **2016**, *162*, 500–510. [[CrossRef](#)] [[PubMed](#)]

25. Posa, V.R.; Annavaram, V.; Koduru, J.R.; Ammireddy, V.R.; Somala, A.R. Graphene-ZnO nanocomposite for highly efficient photocatalytic degradation of methyl orange dye under solar light irradiation. *Korean J. Chem. Eng.* **2016**, *33*, 456–464. [[CrossRef](#)]
26. Nenavathu, B.P.; Kandula, S.; Verma, S. Visible-light-driven photocatalytic degradation of safranin-T dye using functionalized graphene oxide nanosheet (FGS)/ZnO nanocomposites. *RSC Adv.* **2018**, *8*, 19659–19667. [[CrossRef](#)]
27. Yaqoob, A.A.; Mohd Noor, N.H.B.; Serrà, A.; Mohamad Ibrahim, M.N. Advances and challenges in developing efficient graphene oxide-based ZnO photocatalysts for dye photo-oxidation. *Nanomaterials* **2020**, *10*, 932. [[CrossRef](#)]
28. Raizada, P.; Sudhaik, A.; Singh, P. Photocatalytic water decontamination using graphene and ZnO coupled photocatalysts: A review. *Mat. Sci. Energy Technol.* **2019**, *2*, 509–525. [[CrossRef](#)]
29. Rathnasamy, R.; Thangasamy, P.; Thangamuthu, R.; Sampath, S.; Alagan, V. Green synthesis of ZnO nanoparticles using Carica papaya leaf extracts for photocatalytic and photovoltaic applications. *J. Mater. Sci. Mater. Electron.* **2017**, *28*, 10374–10381. [[CrossRef](#)]
30. Wang, Q.; Mei, S.; Manivel, P.; Ma, H.; Chen, X. Zinc oxide nanoparticles synthesized using coffee leaf extract assisted with ultrasound as nanocarriers for mangiferin. *Curr. Res. Nutr. Food Sci.* **2022**, *5*, 868–877. [[CrossRef](#)]
31. Koupaei, M.H.; Shareghi, B.; Saboury, A.A.; Davar, F.; Semnani, A.; Evini, M. Green synthesis of zinc oxide nanoparticles and their effect on the stability and activity of proteinase K. *RSC Adv.* **2016**, *6*, 42313–42323. [[CrossRef](#)]
32. Qu, J.; Yuan, X.; Wang, X.; Shao, P. Zinc accumulation and synthesis of ZnO nanoparticles using *Physalis alkekengi* L. *Environ. Pollut.* **2011**, *159*, 1783. [[CrossRef](#)] [[PubMed](#)]
33. Qu, J.; Luo, C.; Hou, J. Synthesis of ZnO nanoparticles from Zn-hyperaccumulator (*Sedum alfredii* Hance) plants. *Micro. Nano Lett.* **2011**, *6*, 174. [[CrossRef](#)]
34. Singh, J.; Dutta, T.; Kim, K.-H.; Rawat, M.; Samddar, P.; Kumar, P. ‘Green’ synthesis of metals and their oxide nanoparticles: Applications for environmental remediation. *J. Nanobiotechnol.* **2018**, *16*, 84. [[CrossRef](#)] [[PubMed](#)]
35. Dikshit, P.K.; Kumar, J.; Das, A.K.; Sadhu, S.; Sharma, S.; Singh, S.; Gupta, P.K.; Kim, B.S. Green synthesis of metallic nanoparticles: Applications and limitations. *Catalysts* **2021**, *11*, 902. [[CrossRef](#)]
36. Sharma, D.; Sabela, M.I.; Kanchi, S.; Bisetty, K.; Skelton, A.A.; Honarparvar, B. Green synthesis, characterization and electrochemical sensing of silymarin by ZnO nanoparticles: Experimental and DFT studies. *J. Electroanal. Chem.* **2018**, *808*, 160–172. [[CrossRef](#)]
37. Wojnarowicz, J.; Opalinska, A.; Chudoba, T.; Gierlotka, S.; Mukhovskiy, R.; Pietrzykowska, E.; Sobczak, K.; Lojkowski, W. Effect of water content in ethylene glycol solvent on the size of ZnO nanoparticles prepared using microwave solvothermal synthesis. *J. Nanomater.* **2016**, *1*, 2016. [[CrossRef](#)]
38. Tariq, M.; Khan, A.U.; Rehman, A.U.; Ullah, S.; Jan, A.U.; Khan, Z.U.; Muhammad, N.; Islam, Z.U.; Yuan, Q. Green synthesis of ZnO@GO nanocomposite and its efficient antibacterial activity. *Photodiagn. Photodyn. Ther.* **2021**, *35*, 102471. [[CrossRef](#)]
39. Sharma, A.; Sharma, R.; Sharma, M.; Kumar, M.; Barbhai, M.D.; Lorenzo, J.M.; Sharma, S.; Samota, M.K.; Atanassova, M.; Caruso, G.; et al. *Carica papaya* L. leaves: Deciphering its antioxidant bioactives, biological activities, innovative products, and safety aspects. *Oxid. Med. Cell. Longev* **2022**, *2022*, 2451733. [[CrossRef](#)]
40. Goswami, S.; Banerjee, P.; Datta, S.; Mukhopadhyay, A.; Das, P. Graphene oxide nanoplatelets synthesized with carbonized agro-waste biomass as green precursor and its application for the treatment of dye rich wastewater. *Process Saf. Environ. Prot.* **2017**, *106*, 163–172. [[CrossRef](#)]
41. Shams, S.S.; Zhang, L.S.; Hu, R.; Zhang, R.; Zhu, J. Synthesis of graphene from biomass: A green chemistry approach. *Mater. Lett.* **2015**, *161*, 476–479. [[CrossRef](#)]
42. Yaqoob, A.A.; Ibrahim, M.N.M.; Yaakop, A.S.; Umar, K.; Ahmad, A. Modified graphene oxide anode: A bioinspired waste material for bioremediation of Pb<sup>2+</sup> with energy generation through microbial fuel cells. *Chem. Eng. J.* **2021**, *417*, 128052. [[CrossRef](#)]
43. Štengl, V.; Bakardjieva, S.; Murafa, N. Preparation and photocatalytic activity of rare earth doped TiO<sub>2</sub> nanoparticles. *Mater. Chem. Physics.* **2009**, *114*, 217–226. [[CrossRef](#)]
44. Raza, W.; Khan, A.; Alam, U.; Muneer, M.; Bahnmann, D. Facile fabrication of visible light induced Bi<sub>2</sub>O<sub>3</sub> nanorod using conventional heat treatment method. *J. Mol. Struct.* **2016**, *1107*, 39–46. [[CrossRef](#)]
45. Faramawy, A.; Elsayed, H.; Scian, C.; Mattei, G. Structural, optical, magnetic and electrical properties of sputtered ZnO and ZnO:Fe thin films: The role of deposition power. *Ceramics* **2022**, *5*, 1128–1153. [[CrossRef](#)]
46. Agami, W.R.; Faramawy, A.M. Influence of Gd<sup>3+</sup> substitution and preparation technique on the optical and dielectric properties of Y<sub>3</sub>Fe<sub>5</sub>O<sub>12</sub> garnet synthesized by standard ceramic and coprecipitation methods. *J. Mater. Sci. Mater.* **2020**, *31*, 11654–11664. [[CrossRef](#)]
47. Umar, K.; Aris, A.; Ahmad, H.; Parveen, T.; Jaafar, J.; Majid, Z.A.; Reddy, A.; Talib, J. Synthesis of visible light active doped TiO<sub>2</sub> for the degradation of organic pollutants—Methylene blue and glyphosate. *J. Anal. Sci. Technol.* **2016**, *7*, 29. [[CrossRef](#)]
48. Singh, H.; Kumar, A.; Thakur, A.; Kumar, P.; Nguyen, V.-H.; Vo, D.-V.N.; Sharma, A.; Kumar, D. One-pot synthesis of magnetite-ZnO nanocomposite and its photocatalytic activity. *Top. Catal.* **2020**, *63*, 1097–1108. [[CrossRef](#)]
49. Ramesh, M.; Anbuvaran, M.; Viruthagiri, G. Green synthesis of ZnO nanoparticles using solanum nigrum leaf extract and their antibacterial activity. *Spectrochim. Acta A Mol. Biomol. Spectrosc.* **2015**, *136*, 864–870. [[CrossRef](#)]
50. Chen, Y.L.; Zhang, C.E.; Deng, C.; Fei, P.; Zhong, M.; Su, B.T. Preparation of ZnO/GO composite material with highly photocatalytic performance via an improved two-step method. *Chin. Chem. Lett.* **2013**, *24*, 518–520. [[CrossRef](#)]

51. Khoa, N.T.; Kim, S.W.; Van Thuan, D.; Tien, H.N.; Hur, S.H.; Kim, E.J.; Hahn, S.H. Fast and effective electron transport in a Au–graphene–ZnO hybrid for enhanced photocurrent and photocatalysis. *RSC Adv.* **2015**, *5*, 63964–63969. [[CrossRef](#)]
52. Murali, A.; Sarswat, P.K.; Free, M.L. Minimizing electron-hole pair recombination through band-gap engineering in novel ZnO-CeO<sub>2</sub>-RGO ternary nanocomposite for photoelectrochemical and photocatalytic applications. *Environ. Sci. Pollut. Res.* **2020**, *27*, 25042–25056. [[CrossRef](#)] [[PubMed](#)]
53. Chauhan, H.A.; Rafatullah, M.; Ali, K.A.; Umar, M.F.; Khan, M.A.; Jeon, B.H. Photocatalytic activity of graphene oxide/zinc oxide nanocomposite derived from rice husk for the degradation of phenanthrene under ultraviolet-visible light. *J. Water Process Eng.* **2022**, *47*, 102714. [[CrossRef](#)]

**Disclaimer/Publisher’s Note:** The statements, opinions and data contained in all publications are solely those of the individual author(s) and contributor(s) and not of MDPI and/or the editor(s). MDPI and/or the editor(s) disclaim responsibility for any injury to people or property resulting from any ideas, methods, instructions or products referred to in the content.